Understanding the Regioselectivity of Aromatic Hydroxylation Over Divanadium-Substituted γ-Keggin Polyoxotungstate

Igor Y. Skobelev,[a,b,] Vasiliy Yu. Evtushok,[a,b] Oxana A. Kholdeeva,[a,b] Nataliya V. Maksimchuk,[a,b] Raisa I. Maksimovskaya,[a] Josep M. Ricart,[c] Josep M. Poblet, [c] Jorge J. Carbó[c,]**

[a] Boreskov Institute of Catalysis, Lavrentiev ave. 5, Novosibirsk 630090 (Russia). [b]Novosibirsk State University, Pirogova str. 2, Novosibirsk 630090 (Russia). [c]Department de Química Física i Inorgànica, Universitat Rovira i Virgili, Marcel·lí Domingo 1, 43007 Tarragona (Spain).

KEYWORDS. Aromatic hydroxylation, hydrogen peroxide, homogeneous catalysis, kinetic-modeling, pseudocumene, polyoxometalate, vanadium, DFT

ABSTRACT. The aromatic hydroxylation of pseudocumene (PC) with aqueous hydrogen peroxide catalyzed by the divanadium-substituted γ-Keggin polyoxotungstate $TBA_4[\gamma\text{-}PW_{10}O_{38}V_2(\mu\text{-}O)(\mu\text{-}OH)]$ (TBA-**1H**, TBA = tetrabutylammonium) has been studied using kinetic modeling and DFT calculations. This reaction features high chemoselectivity and unusual regioselectivity, affording 2,4,5-trimethylphenol (TMP) as the main product. Then the computational study was extended to the analysis of the regioselectivity for other alkoxy- and alkylarene substrates. The protonation/deprotonation of TBA-**1H** in MeCN/*t*BuOH (1:1) was

investigated by the ^{31}P NMR spectroscopy. Forms with different protonation state, [γ-$PV_2W_{10}O_{40}]^{5-}$ (**1**), [γ-$HPV_2W_{10}O_{40}]^{4-}$ (**1H**) and [γ-$H_2PV_2W_{10}O_{40}]^{3-}$ (**1H$_2$**), have been identified, and the protonation equilibrium constants were estimated on the basis of the ^{31}P NMR data. DFT calculations were used to investigate the oxygen transfer process from hydroperoxo species, [γ-$PW_{10}O_{38}V_2$(μ-O)(μ-OOH)]$^{4-}$ (**2**) and [γ-$PW_{10}O_{38}V_2$(μ-OH)(μ-OOH)]$^{3-}$ (**2H**), and peroxo complex [γ-$PW_{10}O_{38}V_2$(μ-η^2:η^2-O_2)]$^{3-}$ (**3**) toward the different positions in the aromatic ring of PC, anisole and toluene substrates. Product, kinetic, and computational studies on the PC hydroxylation strongly support a mechanism of electrophilic oxygen atom transfer from peroxo complex **3** to the aromatic ring of PC. The kinetic modeling revealed that contribution of **3** into the initial reaction rate is, on the average, about 70%, but it may depend on the reaction conditions. DFT calculations showed that the steric hindrance exerted by peroxo complex **3** is responsible of the origin of the unusual regioselectivity observed in PC hydroxylation, while for anisole and toluene the regioselective *para*-hydroxylation is due to electronic preference during the oxygen transfer from the active peroxo species **3**.

INTRODUCTION

The selective oxidation of aromatic rings is an important field of both industrial and synthetic chemistry. Substituted phenols are important intermediate products in the polymer processing and production of fine chemicals,[1-3] while quinones are crucial intermediates in the synthesis of essential vitamins, nutraceuticals, and pharmaceuticals.[4-7] During the past decade, a few efficient catalyst systems have been elaborated for the selective oxidation of alkylphenols to quinones using environmentally benign oxidants (O_2, H_2O_2, *t*BuOOH).[8] On the contrary, selective oxygenation of aromatic rings of alkylbenzenes remains one of the most challenging

transformations in the organic synthesis.[9-12] Alkylbenzenes have electron-donating groups that activate the aromatic nucleus toward electrophilic attack, but on the other hand, alkyl substituents are prone to oxidation, which results in poor aromatic oxidation selectivity. Non-catalytic stoichiometric oxidations of arenes with hazardous and toxic reagents, such as CrO_3, MnO_2, OsO_4 and others, are still widely employed in fine organic synthesis.[1,4,5,13] Such processes produce large amounts of inorganic waste contaminated by organic tars. The recently emerged urgency of the economical and environmental sustainability encourages the scientific community to develop catalytic chemical processes, which reduce the burden on the environment.[14-16] In particular, the development and implementation of efficient catalytic systems for the aromatic oxyfunctionalization of alkylsubstituted arenes using hydrogen peroxide as the green oxidant is a challenging goal of modern catalysis.

Aromatic oxidation of 1,2,4-trimethylbenzene or pseudocumene (PC) to 2,3,5-trimethyl-1,4-benzoquinone (TMBQ, vitamin E key intermediate) is considered as *in posse* industrial process[17]. Currently, TMBQ is produced on industrial scale through oxidation of 2,3,6- and 2,3,5-trimethylphenols (TMP).[8,18-20] In contrast to the oxidation of TMP, the direct aromatic oxidation of PC has been scarcely described in the literature.9 Few non-catalytic procedures with *meta*-chloroperoxybenzoic acid[21] and H_2O_2/HCOOH mixture[22] as oxidants have been reported. Beller and co-workers suggested use of iron complexes as catalysts for aromatic oxidations with hydrogen peroxide.[18] So far, methylrhenium trioxide seems to be the most efficient catalyst for H_2O_2-based oxidation of PC.[17,23,24]

Early-transition-metal-oxygen anionic clusters or polyoxometalates (POMs for short) are known as versatile catalysts for a wide range of liquid-phase oxidations.[25,26,27,28,29] While many POMs catalyze heterolytic activation of H_2O_2 and oxygen atom transfer to alkenes and thioethers, thus

far only one POM, i.e. the divanadium substituted γ-Keggin phosphotungstate $(Bu_4N)_4[\gamma\text{-}PW_{10}O_{38}V_2(\mu\text{-}O)(\mu\text{-}OH)]$ (designated as TBA-**1H**, where TBA stands for tetrabutylammonium) (see Scheme 1b), is known as an effective catalyst for aromatic hydroxylation of alkylarenes.[30] The same divanadium-substituted POM had been able to catalyze stereo- and regioselective hydroxylation of alkanes with H_2O_2.[31] Moreover, some of us have found that TBA-**1H** catalyzes effectively oxidation of various alkylated phenols/naphtols[32] and methoxyarenes[33] to the corresponding *p*-benzo/naphthoquinones, outperforming the divanadium-substituted silicotungstate $(Bu_4N)_4H_2[\gamma\text{-}SiW_{10}V_2O_{40}]$ and dititanium-substituted silicotungstate $(Bu_4N)_8[\{\gamma\text{-}SiW_{10}Ti_2O_{36}(OH)_2\}_2(\mu\text{-}O)_2]$ catalysts. Recently, we have also reported that TBA-**1H** is able to catalyze hydroxylation of the aromatic ring of PC.[34] The lack of methyl group oxidation products was consistent with electrophilic hydroxylation mechanism while unusual regioselectivity toward the formation of 2,4,5- and 2,3,5-TMP (ca. 7 : 1 : <0.15, see Scheme 1b) indicated that steric factors may have a strong influence on the oxygen transfer process. In general, it appears that the divanadium substituted γ-Keggin phosphotungstate behaves as a *privileged* catalyst in a range of selective oxidations with the green oxidant H_2O_2 under mild conditions, and therefore, understanding its functioning in detail can contribute to the development of novel effective oxidation processes.

The group of Mizuno revealed that the presence of acid co-catalyst and MeCN/*t*BuOH as solvent is crucial for the catalytic activity of TBA-**1H** in H_2O_2-based oxygenation of alkanes,[31] electron-deficient alkenes,[35] and arenes.[30] In our previous work, we confirmed that the addition of acid co-catalyst and *t*BuOH co-solvent is required for the PC aromatic hydroxylation in the presence of TBA-**1H**.[34] Without $HClO_4$, the yield of TMP attained only 24% after 60 min whereas it reached 64% after 10 min if 1 equiv. of $HClO_4$ (relative to the POM catalyst) was added. Mizuno

suggested that the role of acid in the **1H**-catalyzed oxidations is to form a diprotonated polyoxoanion, $[\gamma\text{-}H_2PV_2W_{10}O_{40}]^{3-}$ (**1H$_2$**) that, upon interaction with H_2O_2, forms hydroperoxo complex $[\gamma\text{-}PW_{10}O_{38}V_2(\mu\text{-}OH)(\mu\text{-}OOH)]^{3-}$ (**2H**), dehydration of which leads to a highly electrophilic peroxo species, $[\gamma\text{-}PW_{10}O_{38}V_2(\mu\text{-}\eta^2\text{:}\eta^2\text{-}O_2)]^{3-}$ (**3**) (Scheme 2).

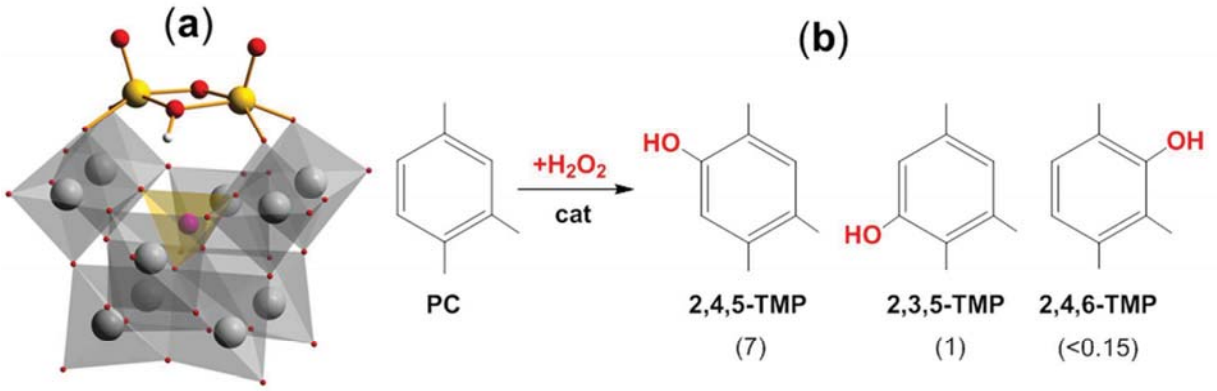

Scheme 1. Molecular structure of species **1H** (a), and possible products of the hydroxylation of pseudocumene with experimental distribution in parenthesis (b).

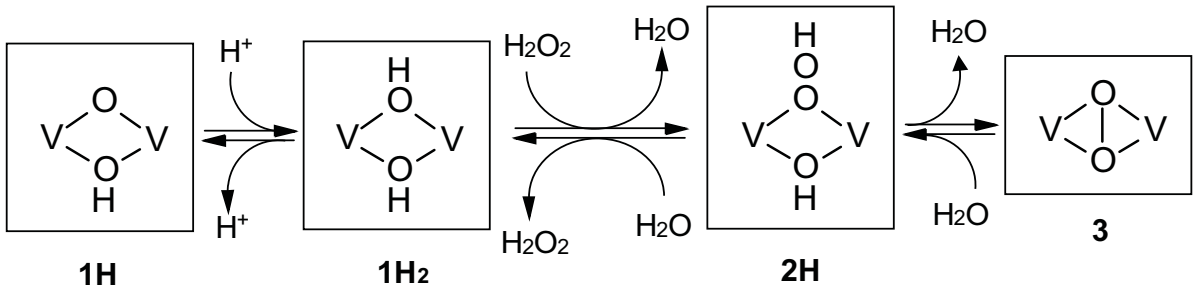

Scheme 2. Tentative mechanism of the formation of active peroxo complex **3**.

Several computational studies were dedicated to characterization of the catalytic activity of the siliceous analog of **1H**, $[\gamma\text{-}SiW_{10}O_{38}V_2(\mu\text{-}OH)(\mu\text{-}OH)]^{4-}$, in epoxidation of olefins with H_2O_2.[36,37] While Nakagawa and Mizuno considered only the $\mu\text{-}\eta^2\text{:}\eta^2$ peroxo complex $[\gamma\text{-}SiW_{10}O_{38}V_2(O_2)]^{4-}$ (**3'**) as a possible origin of the catalytic activity,[36] Kuznetsov et al. analyzed reactivity of the

hydroperoxo species [γ-$SiW_{10}O_{38}V_2$(μ-OH)(μ-OOH)]$^{4-}$ (**2H'**) as well and concluded that peroxo species **3'** is more active than **2H'**.[37] Kamata et al. showed by DFT that the calculated energy barrier of the oxidation of *trans*-2-butene by peroxo complex **3** is higher than the barrier for *cis*-2-butene,[35] which pointed out steric hindrance of **3.** However, it has not been reported yet any computational analysis of either the reactivity of the divanadium-substituted phosphotungstate **1H**/H_2O_2 catalyst system toward substituted arenes or of the regioselectivity of the oxygen transfer process.

In this work, we present a detailed study of the mechanism of the TBA-**1H**-catalyzed aromatic hydroxylation of alkylbenezenes using PC as the model substrate by means of the tools of ^{31}P NMR, kinetic modeling, and DFT calculations, as well as the extension of computational analysis to other alkoxy- and alkylarenes reported in the literature. Our aim was to determine the mechanism of this reaction and to understand the origin of the observed regioselectivity for different aromatic substrates.

EXPERIMENTAL

Materials. Pseudocumene (97+%) was obtained from Aldrich. Acetonitrile (Panreac, HPLC grade) and *t*BuOH (Acros Organics, 99+%) were dried and stored over activated 4 Å molecular sieves. All other compounds were of the best available reagent grade and used without further purification. The concentration of H_2O_2 (ca. 35 wt.% in water) was determined iodometrically prior to use.

Catalysts preparation and characterization. The cesium salt of the dilacunary phosphotungstate Cs_7[γ-$PW_{10}O_{36}$]·xH_2O was synthesized as described in the literature.[38] The tetrabutylammonium salt TBA_4[γ-$HPV_2W_{10}O_{40}$] was prepared according to the general

procedure reported by Kamata et al.[31] with some modifications.[32] The number of acid protons in the TBA salt was corroborated by potentiometric titration with TBAOH (Figure S1 in Supporting Information (SI)). The identity and purity of the POM was confirmed by FTIR (0.5–1.0 wt.% samples in KBr pellets, Agilent 660 FTIR) and multinuclear NMR. IR (cm^{-1}): 1650, 1380, 1100, 1050, 1030, 980, 890, 800, 520, 490 (the corresponding FTIR spectrum is shown in Figure S2 in SI). ^{51}V NMR (dry MeCN): −581 ppm (Figure S3); ^{31}P NMR (dry MeCN): −14.2 ppm. ^{31}P and ^{51}V NMR spectra were recorded on a Brüker AVANCE-400 spectrometer at 161.67 and 105.24 MHz, respectively, using a high-resolution multinuclear probe head. Chemical shifts for P and V, δ, were determined relative to 85% H_3PO_4 and $VOCl_3$, respectively. For convenience, a 0.2 M solution of $H_4PVMo_{11}O_{40}$ in water was used as a secondary external standard for ^{31}P (−3.70 ppm).

^{31}P NMR monitoring of protonation/deprotonation of TBA-1H. The interaction of TBA-**1H** with $HClO_4$ and TBAOH was studied in *t*-BuOH/MeCN (1:1 v/v) solution at room temperature. A 0.01 M solution of TBA-**1H** was placed into a 10 mm o.d. sample tube, and then an appropriate amount of $HClO_4$ or TBAOH (0.1–2.0 equiv. relative to POM) was gradually added and the chemical shift of the POM signal was measured by ^{31}P NMR immediately after the addition and after some time to make sure that the equilibrium had been reached.

Kinetic experiments. Kinetic experiments of PC hydroxylation with H_2O_2 in the presence of TBA-**1H** were carried out in temperature-controlled glass vessels at 40 °C under vigorous stirring (500 rpm). Concentrations of the reactants were varied in the range of [PC] = 0.8–2.4, [H_2O_2] = 0.036–0.180, [TBA-**1H**] = 0.00041–0.0024, [$HClO_4$] = 0.0009–0.0072, and [H_2O] = 0.14–1.14 M. Typically, the reactions were initiated by the addition of H_2O_2 to a mixture containing aromatic substrate, TBA-**1H** catalyst and $HClO_4$ in a solvent mixture MeCN/t-BuOH

(1:1 v/v; the total volume of the reaction mixture was 1 mL). Samples were taken periodically every 8 minutes during the reaction course (average reaction time = 80 minutes) by a syringe, and accumulation of TMP was determined by GC (Chromos GC-1000 equipped with a flame ionization detector and a quartz capillary column BPX5 30 m×0.25 mm) using biphenyl as internal standard. Each experiment was reproduced at least two times. In all experiments, the conversion of PC was in 2-4.5% range.

Kinetic modeling. Initial PC hydroxylation rates were computed as rates of TMP accumulation. The rate law of the PC hydroxylation was derived applying a steady-state approximation to concentrations of all active species. Procedures for calculation of the initial rate of TMP formation and fitting the rates with the derived law were similar to those described by some of us earlier.[39] For the detailed description of the kinetic modeling procedure and derivation of the rate law, see the SI.

Computational details. The DFT analysis of the reaction pathway was carried out with Gaussian09 rev. C01 software.[40] Geometry optimization of reagents, intermediates, transition states and products was made using B3LYP density functional.[41-43] LANL2DZ pseudopotential[44] was used for W and V atoms and 6-31g(d,p) basis set[45-47] was used for all atoms of PC, water and hydrogen peroxide as well as for oxygen atoms directly bonded to V. For other atoms, 6-31g basis set[45] was used. The geometry optimization was full and without any symmetry constrains, and IEFPCM implicit solvation model included in Gaussian09 (solvent – acetonitrile) was used. Such a computational level has been successfully employed in the study of the reactivity of early-transition-metal-oxygen clusters including quantitative agreement with Arrhenius activation energies[48] and kinetic modeling.[39] It is out of the scope of this study to analyze the specific role of solvent mixture, which has been shown to be important in reaction yield, and

countercations. Future computational studies are planned to address these effects using dynamic simulations analogous to those employed in some of our previous studies.[49] Nevertheless, the effect of the dielectric constant on the regioselectivity was tested by repeating the calculations using the dielectric constant of ^{t}BuOH (12.5), and then, averaging the results with those obtained for acetonitrile. The relative free energies for the isomeric transition states of heterolytic oxygen transfer from hydroperoxo species (**TS3**, see below) vary only in 0.1 kcal·mol^{-1}. Thus, the reported values were obtained using only the free energy in acetonitrile in order not to increase the computational cost unnecessarily. The reaction under investigation occurs in the liquid-phase, but Gaussian calculates gas-phase free energies. To take into account the liquid-phase character of the reaction, a translation entropy correction[50] was incorporated to the computed free energy.

RESULTS AND DISCUSSION

^{31}P NMR monitoring of protonation/deprotonation of TBA-1H and evaluation of protonation constants.

It has long been known that protonation of α-Keggin heteropolyanions $[PV_2W_{10}O_{40}]^{5-}$ (in this POM, two vanadium atoms are statistically distributed over 12 positions of the α-Keggin structure) in acidic media causes a high-frequency shift of the ^{31}P NMR signals.[51-53] The same tendency was observed for γ-Keggin polyanion **1.**[30,31] In CH_3CN solutions, TBA-**1H** reveals a ^{31}P NMR signal at δ –(14.2±0.1) ppm.[30,31,35] In turn, a form containing two protons,TBA-**1H$_2$**, is manifested by a ^{31}P NMR signal at δ –13.8.[31,33] A mixture of mono- and diprotonated forms **1H** and **1H$_2$** may give two separate signals in dry diluted MeCN solutions.[33] However, if some water

or *t*BuOH is added, only one averaged signal is observed due to fast proton exchange on the ^{31}P NMR time scale.

Since the presence of *t*BuOH as co-solvent and $HClO_4$ as co-catalyst is crucial to accomplish effectively hydroxylation of alkylbenezenes in the presence of TBA-**1H**,[30,34] we employed ^{31}P NMR to investigate protonation/deprotonation of TBA-**1H** in a mixture of MeCN/*t*BuOH (1:1 v/v) and then used the ^{31}P NMR data (*vide infra*) to evaluate the corresponding protonation constants for **1** and **1H** (Scheme 3).

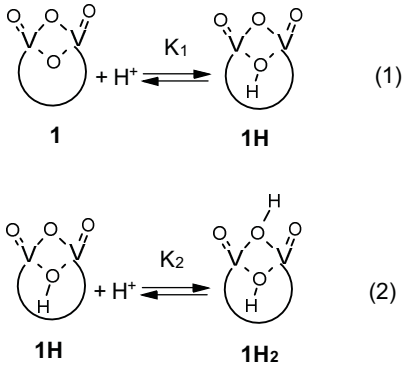

Scheme 3. Protonation equilibriums for species **1** and **1H**.

While the addition of *t*BuOH to MeCN produced insignificant changes in the position of the ^{31}P NMR signal of TBA-**1H**, additives of acid or base resulted in substantial signal shifting. The gradual alterations observed in the ^{31}P NMR spectra of TBA-**1H** upon titration with TBAOH and $HClO_4$ are shown in Figure 1a and Figure 1b, respectively. The ^{31}P signal moved upfield reaching δ –15.0 ppm upon addition of 1 equiv. of TBAOH and then remained constant (Figure 1a), indicating the formation of nonprotonated form **1**. On the contrary, the addition of acid caused a progressive downfield shift of the ^{31}P NMR signal, which attained δ –13.83 ppm at ca.

1 equiv. of H^+ and after that almost did not change (Figure 1b). Note that the chemical shift of –13.8 ppm has been previously assigned to the diprotonated form **1H$_2$**.[31]

Fast exchange on the NMR time scale can be described with a simple formalism[54] using values of chemical shifts of individual forms and protonation equilibrium constants (eq. S1.1 in the SI). Given that, we used the dependences of the ^{31}P chemical shift of TBA-**1H** on the amount of added $HClO_4$ and TBAOH to evaluate the protonation equilibrium constants K_1 and K_2 in MeCN/*t*BuOH (1:1), the solvent mixture that had been identified as optimal for the hydroxylation of alkylbenzenes. Figure S4 shows fitting of the experimental dependences with equation S1.1. The estimated values of K_1 and K_2 equal to $2.5 \cdot 10^5$ and $8.6 \cdot 10^3$ M^{-1} with standard deviations of $1.4 \cdot 10^4$ and $1.5 \cdot 10^2$ M^{-1}, respectively. These values will be used in kinetic modeling of PC oxidation (*vide infra*).

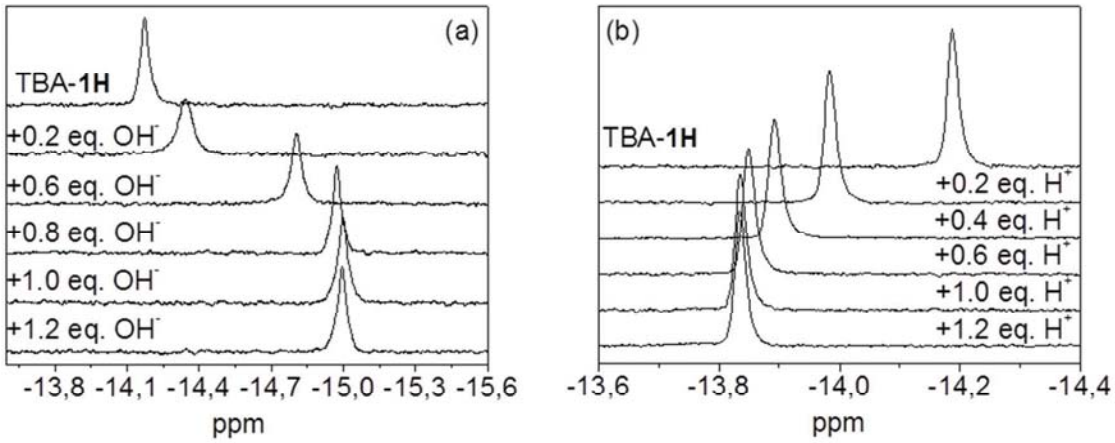

Figure 1. ^{31}P NMR spectra of TBA-**1H** in tBuOH/MeCN (1:1 v/v) upon addition of TBAOH (a) and $HClO_4$ (b).

Kinetics study of PC hydroxylation

Initial rates of TMP formation (W_0) were measured in a wide range of concentrations of all the reagents. Plots of W_0 versus concentrations of water, oxidant, acid, catalyst, and arene are shown in Figure 2 a1–c1 and Figure 3 a1-b1.

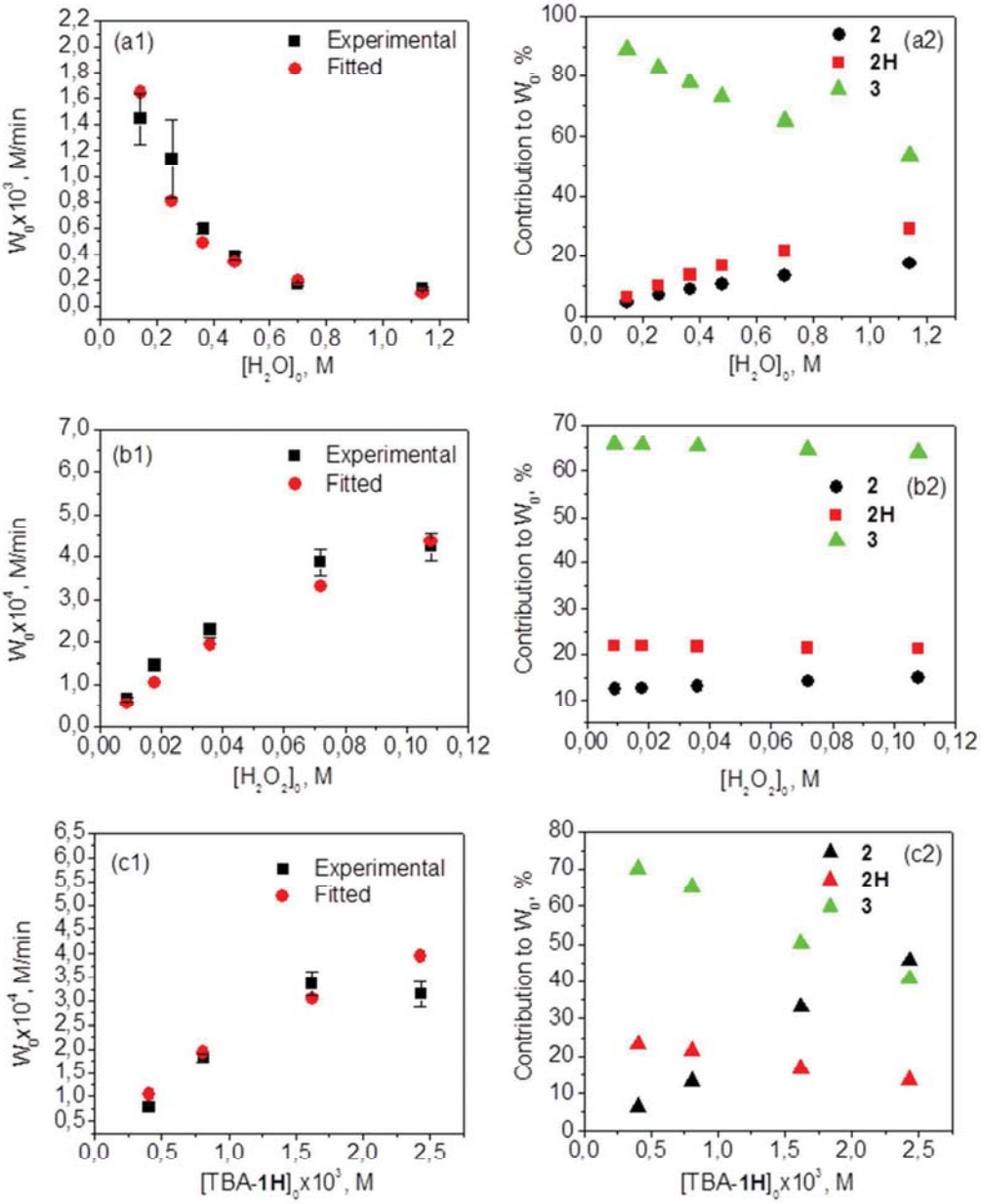

Figure 2. Experimental dependences of initial rates of TMP formation on initial reagent concentrations and their fitting with equation S3.7 (a1–c1) and computed contributions of the active species into the initial reaction rate (a2–c2). Reaction conditions: 0.0081 M TBA-**1H** (a, b), 0.036 M H_2O_2 (a, c), 0.7 M H_2O (b, c), 0.009 M $HClO_4$, 0.8 M PC, 40°C, 1 mL of solvent (MeCN/*t*BuOH = 1:1 v/v).

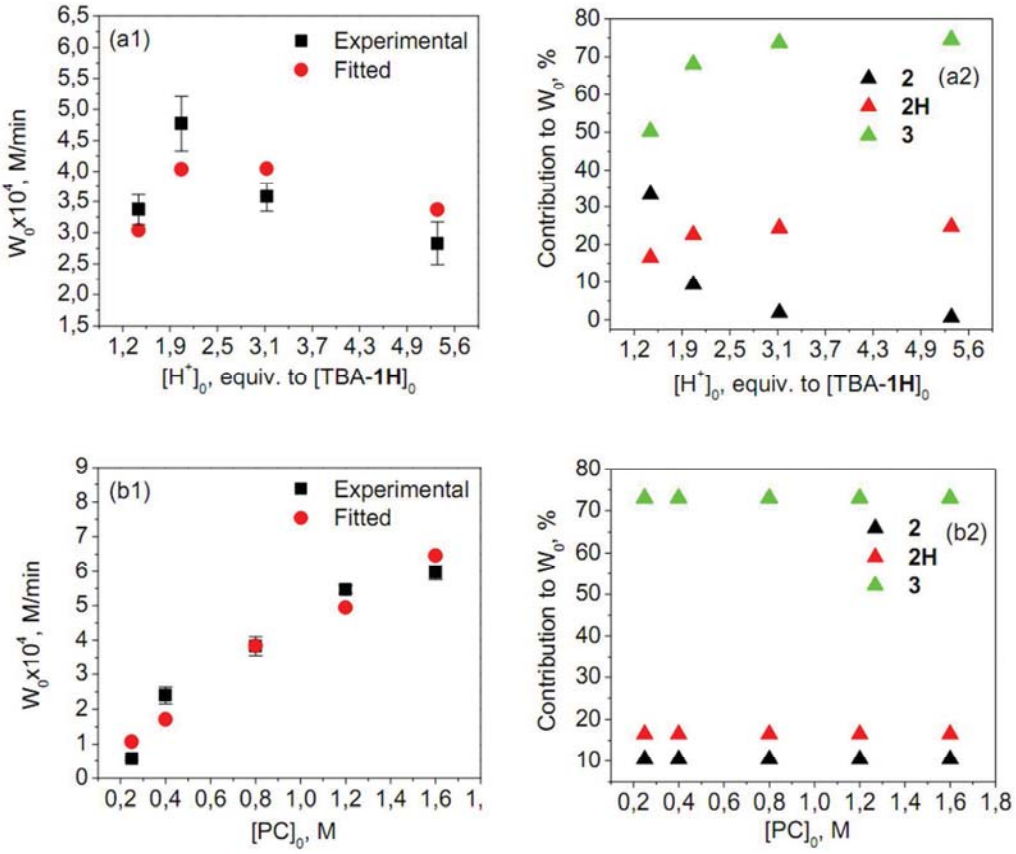

Figure 3. Experimental dependences of initial rates of TMP formation on initial reagent concentrations and their fitting with equation S3.7 (a1–b1) and computed contributions of the active species into the initial reaction rate (a2–b2). Reaction conditions: 0.0162 M TBA-**1H** (a) or 0.0081 M TBA-**1H** (b), 0.036 M H_2O_2, 0.7 M H_2O (a) or 0.48 M H_2O (b), 0.009 M $HClO_4$ (b), 0.8 M PC (a), 40°C, 1 mL of solvent (MeCN/*t*BuOH = 1:1 v/v).

We attempted to rationalize these complicated dependences suggesting a mechanism similar to that proposed by Mizuno[30] that involves the formation of active peroxo species **3**. However, this mechanism has been expanded with an assumption that hydroperoxo complexes [γ-$PW_{10}O_{38}V_2$(μ-O)(μ-OOH)]$^{4-}$ (**2**) and [γ-$PW_{10}O_{38}V_2$(μ-OH)(μ-OOH)]$^{3-}$ (**2H**) might also be able to participate in the hydroxylation process. The protonation equilibria between different forms were also taken into account. The overall reaction mechanism is presented in Scheme 4.

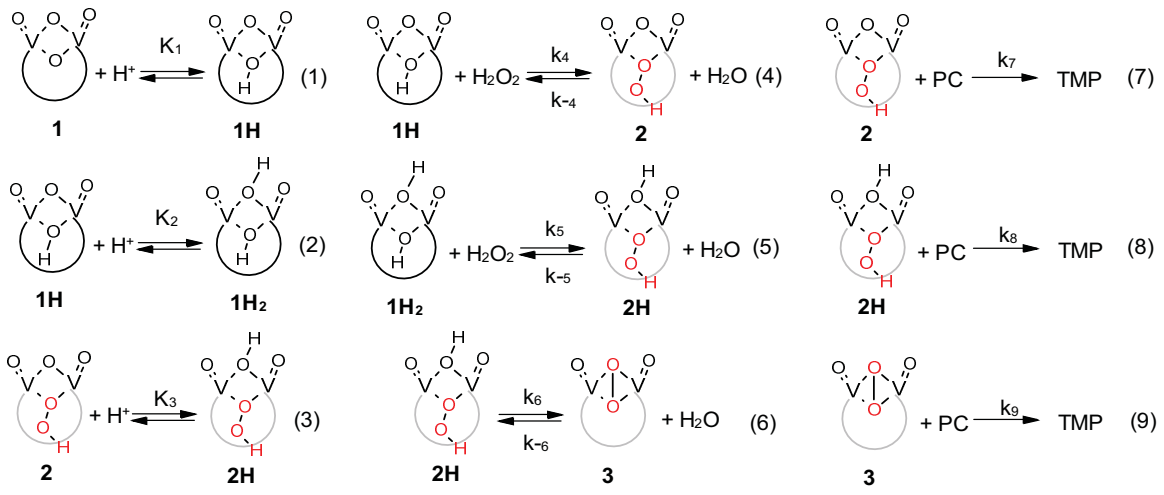

Scheme 4. Proposed mechanism of PC hydroxylation with H_2O_2 in the presence of TBA-**1H**.

By applying a steady-state approximation to concentrations of all active species (**2**, **2H** and **3**), a rate law described by eqs S3.2 and 1 has been drawn (see SI for details). To estimate the corresponding rate and equilibrium constants for the reaction steps depicted in Scheme 4, all the dependencies of the initial reaction rate on reagent concentrations were fitted simultaneously with the rate law derived (Figure 2, a1-c1, and 3 Figure 3, a1–b1). Recently[39], we employed a similar approach for studying mechanism of thioether oxidation with H_2O_2 catalyzed by [(γ-$SiTi_2W_{10}O_{36}(OH)_2)_2(\mu\text{-}O)_2]^{8-}$.

Kinetic regularities mainly reflect the reactivity and concentration of the active species, while the protonation equilibria involve both initial forms of the catalyst, **1**, **1H** and **$1H_2$**, and active peroxo species, **2** and **2H**. The kinetic dependencies themselves are scarcely a good source of data for estimation of protonation equilibrium constants K_1 and K_2 but, fortunately, the values of K_1 and K_2 could be determined independently from the ^{31}P NMR data. To incorporate these values into the kinetic model, we applied a regularization procedure (see SI for details). After modeling with the full parameter set, i.e. with all equilibrium and rate constants for the proposed mechanism (Scheme 4), it was found that concentration of **1** under the experimental conditions employed is very low, so that reaction 1 in Scheme 4 as well as parameter K_1 can be excluded from the kinetic model. The optimal values of k_5 and k_{-5} turned out significantly lower than those of k_4 and k_{-4}, indicating that the formation of **2**, **2H** and **3** mainly proceeds through interaction of **1H** with H_2O_2 (reaction 4 in Scheme 4) while reaction of **$1H_2$** with H_2O_2 (reaction 5 in Scheme 4) is significantly slower. Finally, the following set of parameters was used in the modeling procedure: K_2, K_3, K_6, k_4, k_{-4}, k_7, k_8, and k_9, where $K_6 = k_6/k_{-6}$. To calculate the value of the initial reaction rate with eq. 1 it is necessary to know some additional quantities (eq. 2) which, in turn, depend from the rate and equilibrium constants, initial concentration of reagents and from equilibrium concentration of protons. The latter can be obtained from simultaneous solution of material balance eqs. 3 and 4. The optimal values of all the parameters of eqs. 1 and 2 are given in Table 1.

$$W_0 = \frac{(k_7 + K_3[H^+](k_8 + \alpha_3 k_9))\alpha_2[POM]_0[PC]_0}{\Phi_{POM}} \quad (1)$$

$$\alpha_2 = \frac{k_4[H_2O]_0[H_2O_2]_0}{k_{-4}[H_2O]_0^2 + k_9 K_6 K_3[H^+][PC]_0} \qquad \alpha_3 = \frac{K_6}{[H_2O]_0} \quad (2)$$

$$[H^+]_0 = [H^+] + [\mathbf{1H}](1 + 2K_2[H^+] + \alpha_2(1 + 2K_3[H^+](1 + \alpha_3))) \quad (3)$$

$$[POM]_0 = [\mathbf{1H}](1 + K_2[H^+] + \alpha_2(1 + K_3[H^+](1 + \alpha_3))) = [\mathbf{1H}]\Phi_{POM} \quad (4)$$

Table 1. Optimal parameters of the kinetic model (eqs. 1-2) and their standard deviations.

Parameter	Value	Standard deviation
K_2, M^{-1}	$8.9 \cdot 10^3$	$1 \cdot 10^2$
K_3, M^{-1}	$2.0 \cdot 10^5$	$3 \cdot 10^4$
K_6, M	$9.4 \cdot 10^{-3}$	$1 \cdot 10^{-3}$
k_4, $(M \cdot min)^{-1}$	$9.2 \cdot 10^2$	90
k_{-4}, $(M \cdot min)^{-1}$	$4.0 \cdot 10^3$	$6 \cdot 10^2$
k_7, $(M \cdot min)^{-1}$	9.3	$6 \cdot 10^{-1}$
k_8, $(M \cdot min)^{-1}$	$4.3 \cdot 10^{-1}$	$5 \cdot 10^{-2}$
k_9, $(M \cdot min)^{-1}$	92	10

One may conclude from the data given in Table 1 that peroxo complex **3** is the most active form of the catalyst since the value of the rate constant k_9 (92 $(M \cdot min)^{-1}$) is the highest among constants k_7–k_9. This fact is consistent with the hypothesis proposed by Mizuno that namely peroxo species **3** is responsible for the catalytic activity of TBA-**1H** in aromatic hydroxylation[30]. A contribution of each peroxo species into the overall initial rate of TMP formation can be estimated from the kinetic modeling (eq. S3.8–S3.10, see SI). Although the ratio of all the peroxo species depends on the reaction conditions (Figure 2, a2-c2, and Figure 3, a2–b2), peroxo complex **3** usually predominates and its contribution is about 70% in a wide range of reagent

concentrations (Figure 2, b2, and Figure 3, a2–b2). Average contributions of **2H** and **2** are 21% and 9%, respectively.

While varying the concentration of water, the contribution of peroxo complex **3** changed from 90% ([H_2O] = 0.14 M) to 50% ([H_2O] = 1.14 M). This is consistent with the proposed scheme of the formation of **3** *via* dehydration of **2H** (reaction 6 in Scheme 4). Since the assessment of the rate constants showed that **3** is the most active form, the decrease in its contribution into the oxidation process leads to the reduction of the overall reaction rate (Figue2, a1). The other reason of the observed decrease in the reaction rate is that the increase in water concentration generally disfavors the formation of the active species. Obviously, the contribution of **3** into the initial reaction rate also decreased with increasing concentration of TBA-**1H** (Figure 2, c2).

A complex behavior of the system was observed when the concentration of acid co-catalyst was varied. The experimental dependence of the initial reaction rate on the concentration of acid went through a maximum, which was also reproduced by the kinetic model (Figure 3, a1). Such a behavior may result from a complex equilibrium between all forms of the catalyst. At a low concentration of acid, the concentration of **3** may decrease because it is generated from the protonated form **2H**. Note that **2** gives a significant contribution to the reaction rate when the concentration of acid is low (Figure 3, a2). When the concentration of acid increases, the concentrations of **2H** and **3** also enlarge as well as their contribution into the reaction rate, and then the reaction rate reaches its maximum (Figure 3, a1–a2). However, further increase in the concentration of acid leads to decreasing concentration of **1H**, the main form that participates in the formation of the active peroxo species upon interaction with H_2O_2, which, in turn, results in decreasing concentration of the active species. Consequently, the overall reaction rate decreases (Figure 3, a1) while the individual contributions of the peroxo species into the reaction rate

remain constant (Figure 3, a2). The augmentation of the PC concentration leads to the increase in the reaction rate (Figure 3, b1), which is consistent with the proposed mechanism of the interaction of the active species with PC (Scheme 4). Therefore, the reaction mechanism depicted in Scheme 4 has led to the rate law which is fully consistent with all the kinetic regularities observed experimentally for PC hydroxylation with H_2O_2 catalyzed by TBA-**1H** in the presence of acid co-catalyst.

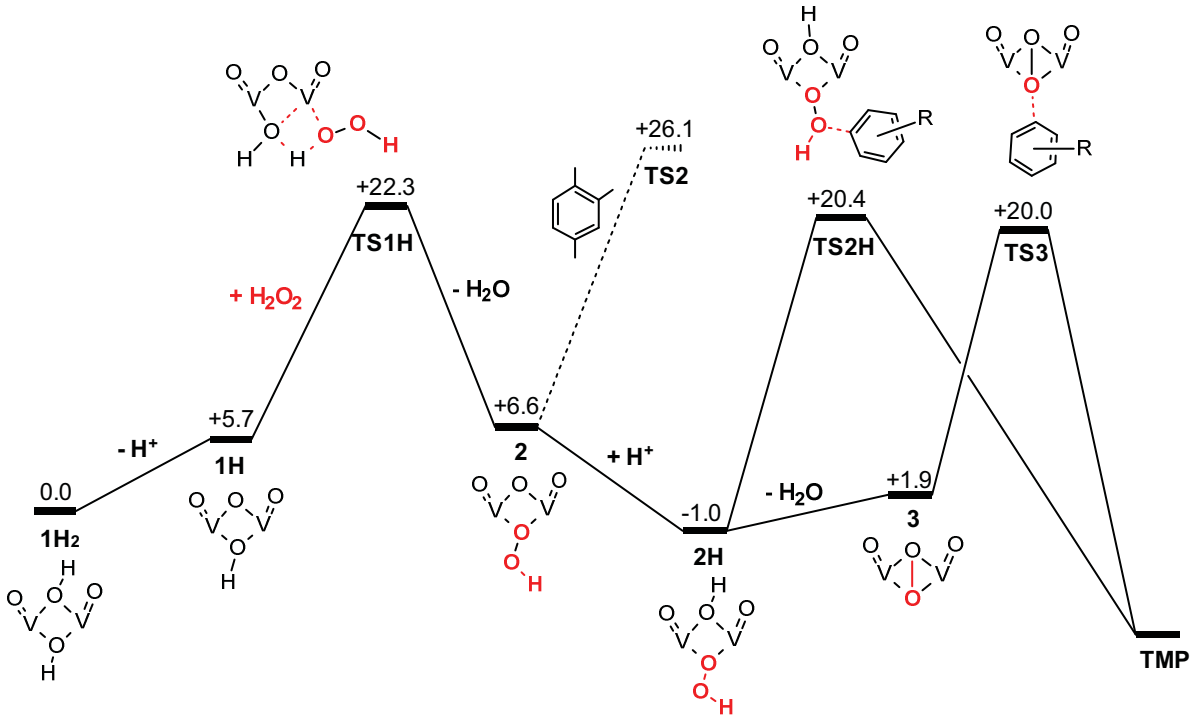

Figure 4. Potential energy profile (kcal·mol^{-1}) for **1H**-catalyzed hydroxylation of PC to TMP derived from kinetic modeling**.**

DFT study of PC hydroxylation

Figure 4 shows the energy profile for PC hydroxylation catalyzed by divanadium-substituted γ-Keggin polyoxotungstate derived from the kinetic modeling using the transition state theory.[39] The mechanism can be divided in three main steps: (1) H_2O_2 activation to form the vanadium

hydroperoxo species **2**, which protonates to yield **2H**, (2) dehydration of **2H** to vanadium peroxo species **3**, which is somewhat endothermic, and (3) electrophilic oxygen transfer from the peroxo species **3**, which is preferred to vanadium hydroperoxo path through species **2H**. This proposal is consistent with the previously DFT-characterized mechanism of a related process, the epoxidation of alkenes by $[\gamma\text{-}H_2SiV_2W_{10}O_{40}]^{4-}$ anion.[36,37]

Table 2. Evaluated from kinetic modeling and calculated free-energy barriers (kcal·mol^{-1}) for oxygen transfer from **2H** and **3** to PC.[a]

	2H	**3**
$\mathbf{\Delta G^{\neq}_{kin.\ mod.}}$	21.4	18.1
$\mathbf{\Delta G^{\neq}_{DFT}}$	24.2	21.3
$\mathbf{\Delta G^{\neq}_{DFT\text{-}corr}}$	19.7	16.8

[a] The $\Delta G^{\neq}_{DFT}$ and $\Delta G^{\neq}_{DFT\text{-}corr}$ values represent uncorrected and corrected free energy barriers, respectively.

In order to understand the origin of the unusual regioselectivity in the **1H**-catalyzed aromatic hydroxylation, we carried out DFT calculations on the electrophilic oxygen transfer from **2H** and **3** to PC substrate. We did not consider the reaction path through hydroperoxo species **2** because, according to the kinetic modeling, it has the highest energy barrier (+26.1 kcal·mol^{-1}) and the lowest contribution into the initial reaction rate (9%, see above). Table 2 collects the computed and evaluated from kinetic modeling free energy barriers of the lowest energy paths for oxygen transfer, while Figure 5 shows the geometries of the corresponding transition states. Since calculated Gibbs free energies overestimate the translational entropy loss in the associative processes, we corrected them by applying Whitesides' correction[50] ($\Delta G^{\neq}_{DFT\text{-}corr}$) and provide both uncorrected and corrected values in Table 2. It is important to note that the entropy correction is

less accurate for protic solvents, and especially, for water. However, the combination of corrected and uncorrected values is informative because it provides a lower and upper limit of entropy loss in associative processes, such as the intermolecular attack of arene to POM active intermediates. Importantly, the values of the two experimental energy barriers lay within the energy range defined by the calculations (see Table 2). Also in agreement with the experimental values, the computed free energy barrier of oxygen transfer decreases on going from hydroperoxo **2H** to peroxo **3** (2.9 kcal·mol^{-1} by DFT *vs.* 3.3 kcal·mol^{-1} experimentally). These results mutually support each other, confirming the characterization of the mechanism by kinetic modeling and DFT calculations.

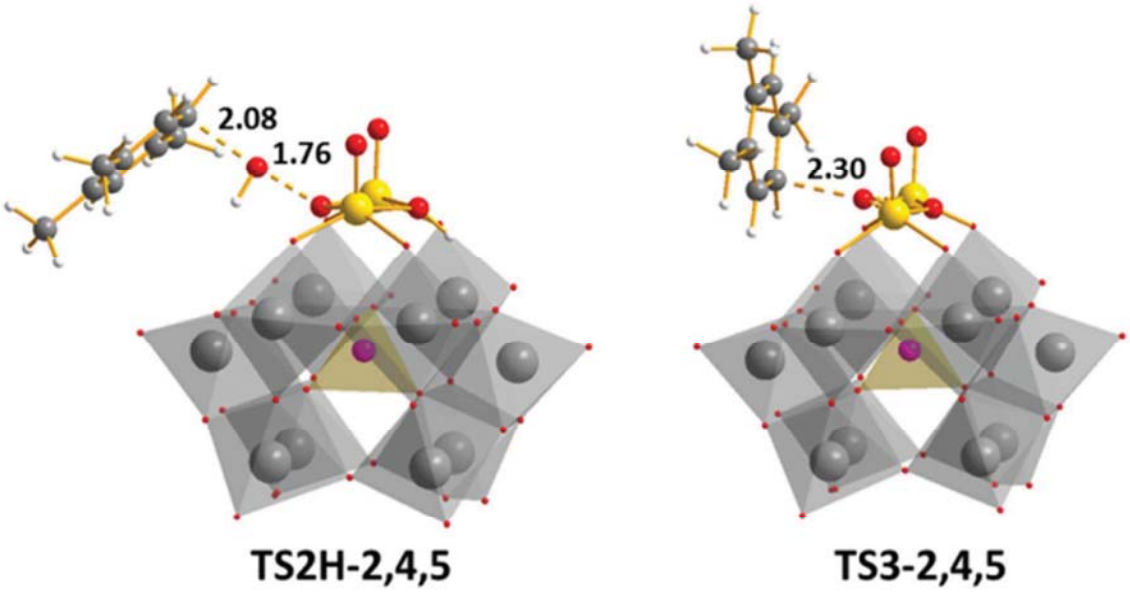

Figure 5. Representation of the DFT computed transition states for oxygen transfer from hydroperoxo complex **2H** and peroxo complex **3** to PC. Selected, lowest-energy regioisomers. Distances in Å**.**

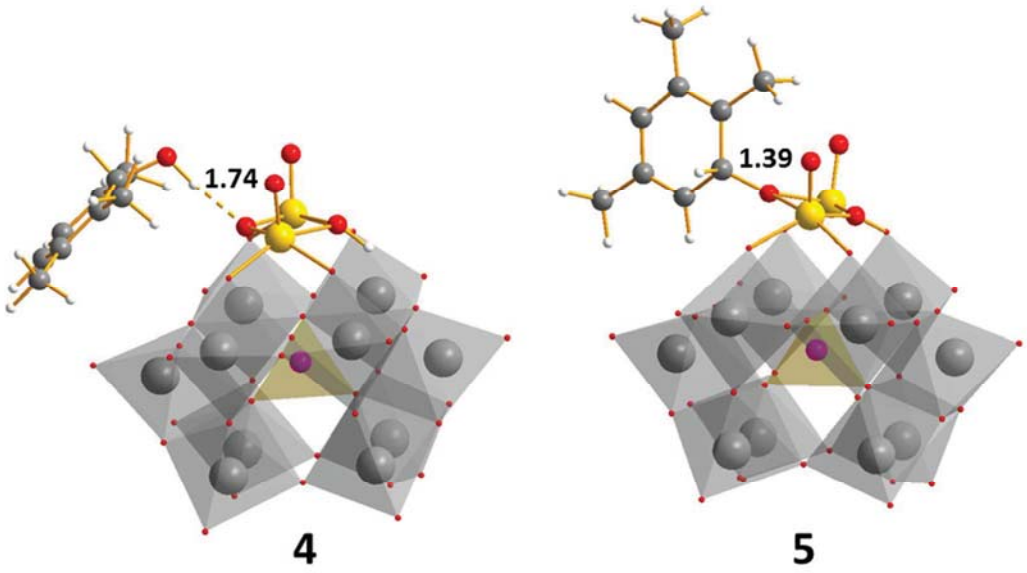

Figure 6. Representation of the DFT computed structures of intermediates obtained after oxygen transfer for hydroperoxo and peroxo paths, **4** and **5**, respectively. Distances in Å**.**

The transition states **TS2H** (Figure 5 and S5) involve the transfer of the O_β–H group to PC from the bridging vanadium hydroperoxo group, yielding a protonated TMP molecule that remains hydrogen-bonded to the $V_2(\mu$-O) group of the POM framework as shown by structure **4** in Figure 6. Then the H-bonded hydrogen can return to the $V_2(\mu$-O) oxo group to recover catalyst **1H2** while the other proton rearranges to form the final TMP product. In fact the same mechanism was proposed for direct conversion of benzene to phenol catalyzed by the enzyme cytochrome P450 on the basis of DFT calculations.[55] Alternatively, the transfer of the O_β–H group to PC might induce a direct proton release from the aromatic ring to a proton acceptor solvent molecule via a classical *SN2* aromatic substitution mechanism. However, the analysis of the role of explicit solvent for the minor reaction path is besides of the scope of this study. Analyzing in more detail the preferred peroxo path, we found that the transition state **TS3-2,3,5** leads to a μ-alkoxo divanadium intermediate (**5**) with the new C–O bond lengthening 1.39 Å (see Figure 6), which

free-energy is 21.3 kcal.mol^{-1} bellow reactants. Thus, calculations indicate that the formation of **5** is irreversible (reverse free-energy barrier $\Delta G^{\neq}_{\mathbf{5}\rightarrow\mathbf{TS3}} \cong 40$ kcal·mol^{-1}) and, consequently, that the electrophilic oxygen transfer is the selectivity-determining step. From **5**, the free-energy barrier associated to proton rearrangement to give the final TMP product is 24.7 kcal·mol^{-1}, that is feasible for a reaction occurring at 40ºC.

Table 3. Calculated relative free energies (kcal·mol^{-1}) for the isomeric transition states of heterolytic oxygen transfer from **3** and **2H** to PC and relative free energies (kcal·mol^{-1}) of the protonated PC substrate.

Isomer	**$\Delta\Delta G^{\neq}$ (TS3)**	**$\Delta\Delta G^{\neq}$ (TS2H)**	**$\Delta\Delta G$ (PC+H$^+$)**
2,4,5	0.0	+0.3	0.0
2,3,5	+0.6	+3.3	+3.1
2,3,6	+5.7	0.0	+0.2

Table 3 (second column) collects the relative free energies of the different isomeric transition states leading to 2,4,5-, 2,3,5- and 2,3,6-TMP isomers through the preferred peroxo path (**TS3**). The results are consistent with the unusual regioselectivity toward 2,4,5- and 2,3,5-TMP isomers (ca. 7:1) that was observed in PC hydroxylation in the presence of TBA-**1H**.[34] The computed lowest energy path corresponds to **TS3-2,4,5** followed at relatively low energy (0.6 kcal.mol^{-1}) by **TS3-2,3,5** path. This energy difference is qualitatively close to that expected from the observed isomer ratio at 40º C, i.e., 1.2 kcal·mol^{-1}. The **TS3-2,3,6** path is significantly higher in energy (5.7 kcal·mol^{-1}) and no reaction is expected to occur through this pathway. Since hydroperoxo path (**TS2H**) has a minor contribution to final product distribution (see above), we can conclude that calculations reproduce qualitatively the preferred formation of 2,4,5-TMP

product, although the quantitative prediction of the distribution of isomers (specially of the minor ones) is not very accurate.

Origin of the unusual regioselectivity of PC hydroxylation: steric *vs* electronic preference

In the peroxo path (**TS3**), the product distribution differs from the hydroperoxo path (**TS2H**), which might explain the origin of the unusual regioselectivity (see Table 3). We propose that the regioselectivity switch from its electronic preference due to the steric factors governing the interaction between the substrate and the POM framework. In fact, Mizuno and co-workers have demonstrated that the calculated energy barrier of epoxidation of *cis*-2-butene by peroxo complex **3** is lower than that of *trans*-2-butene,[35] indicating crucial importance of steric factor for the reactivity of **3**. Also, we have shown that other POM structures such as the dititanium-substituted sandwich anion determines the selectivity in the epoxidation of alkenes via a similar steric effect.[56,57] To evaluate the electronic preference toward electrophiles of the different carbon sites of PC, their affinity towards protonation was investigated. The relative free energies of protonated PC species are shown in Table 3. They follow roughly the same trend as oxygen transfer from the O_β oxygen of the hydroperoxo group (**TS2H**), for which there is no sterical hindrance. Conversely, in peroxo intermediate **3**, the oxygen transfer occurs closer to the POM framework and steric repulsion with the substrate comes into play. Consequently, the most hindered position with methyl substituents at the two alpha positions, **TS3-2,3,6**, becomes the highest in energy. The lowest energy isomeric transitions states are **TS3-2,4,5** and **TS3-2,3,5**, which are 5.7 and 5.1 kcal·mol^{-1} lower than **TS3-2,3,6**, while the atomic charges, determined with the CHELPG method, at the C5 and C6 carbons of PC (-.22 and -.17 a.u., respectively) are less negative that that at the C3 carbon (-.29 a.u.). Therefore, the positions C5 and C6, although less nucleophilic, have less sterical hindrance with the POM framework and consequently

become favorable, thereby switching the electronically-driven regioselectivity (TMP-2,3,6) usually observed in the oxidations of PC to the sterically-driven one (TMP-2,4,5). For hydroperoxo species **2H**, free energies of **TS2H-2,3,6** and **TS2H-2,4,5** (Table 3) are similar, which implies that the formation of 2,3,6- and 2,4,5-TMP might be a competitive process. However, only minor amounts of 2,3,6-TMP were detected in the experimental study of PC hydroxylation,[34] which is consistent with the low (~21%) contribution of **2H** into the initial aromatic hydroxylation rate. Therefore, the DFT study pointed out that the steric hindrance exerted by peroxo complex **3** during electrophilic oxygen transfer is responsible of the origin of the unusual regioselectivity observed in PC hydroxylation over TBA-**1H**.

Origin of regioselectivity in hydroxylation of alkoxy- and alkylarene substrates

Once we have characterized the mechanism and identified the regioselectivity-determining species for the aromatic hydroxylation using pseudocumene as a model substrate, we analyze whether this mechanism can be also used to explain the unique regioselectivity exhibited by divanadium-substituted phosphotungstate $\mathbf{1H_2}$ in the direct hydroxylation of various arenes with H_2O_2 reported recently by Mizuno *et al.*[30] To this end, we select two experimentally tested monosubstituted substrates, anisole as representative of alkoxyarenes and toluene as representative of alkylarenes (Scheme 5). For both substrates, the free-energy barrier of the peroxo path (**3** + arene → $\mathbf{TS3_{ar}}$: 17.4 and 20.5 kcal·mol^{-1} for anisole and toluene, respectively) is significantly lower than that of the hydroperoxo path (**2H** + arene → $\mathbf{TS2H_{ar}}$: 22.5 and 28.2 kcal·mol^{-1}, respectively). Thus the peroxo complex **3** is the active species mainly responsible of the oxygen transfer to the substrate.

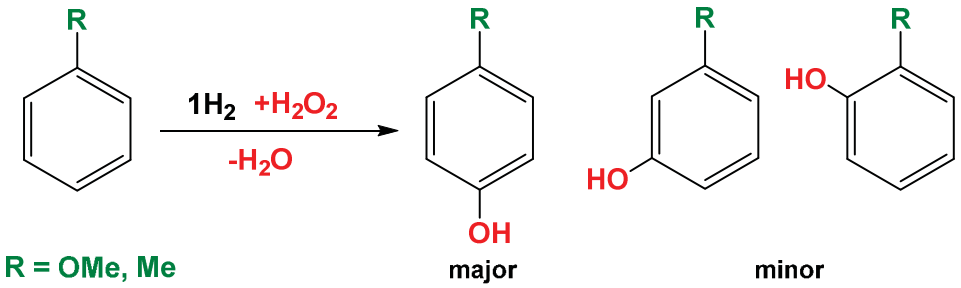

Scheme 5. Hydroxylation of alkoxy- and alkylarenes with H_2O_2 catalyzed by divanadium-substituted phosphotungstate $\mathbf{1H_2}$.

Table 4. Calculated relative free energies (kcal·mol^{-1}) for the isomeric transition states of heterolytic oxygen transfer from **2H** and **3** to anisole and toluene, and comparison between computational and experimental regioselectivities (%).

compound	isomer	$\Delta\Delta G^{\neq}$ (TS2H$_{ar}$)	$\Delta\Delta G^{\neq}$ (TS3$_{ar}$)	% selec. (calc.)	% selec. (exp.)
anisole	*ortho*	1.2	1.0	18	5
	meta	5.9	5.2	<1	<1
	para	0.0	0.0	82	95
toluene	*ortho*	-1.6	2.8	1	7
	meta	1.2	1.1	16	16
	para	0.0	0.0	83	77

Table 4 collects the relative free-energies of the isomeric transition states for oxygen transfer through hydroperoxo (**TS2H$_{ar}$**) and peroxo (**TS3$_{ar}$**) paths. Importantly, there is an excellent agreement between the experimental regioselectivities and those predicted from the relative free-energies of the peroxo path, **TS3$_{ar}$** (see Table 4). Calculations do not only reproduce the preference for the *para* isomer but also the relative distribution between the *ortho* and *meta* isomers. This correspondence between experimental and computational regioselectivities further

supports that the oxygen transfer form peroxo complex **3** is the key regioselectivity-determining step. The comparison of the relative free-energies for peroxo (**TS3$_{ar}$**) path with those of hydroperoxo (**TS2H$_{ar}$**) can be used to evaluate the steric and electronic effects on the regioselectivity (see Table 4). In the case of anisole the distribution of transition state energies is almost identical for **TS3$_{ar}$** and **TS2H$_{ar}$** paths, indicating that the regioselectivity is governed by the electronic preference of the substrate. We recall that in **TS2H$_{ar}$** the oxygen transfer occurs farther from the POM framework than in **TS3$_{ar}$**. For toluene the distribution of the minor regioisomers is slightly different from anisole with observable amounts of the *meta*-substituted product. Comparing peroxo (**TS3$_{ar}$**) and hydroperoxo (**TS2H$_{ar}$**) transition states, we found that the relative energies of *meta*/*para* regioisomers are almost identical indicating an electronic control in their relative orientation. On the other hand, the *ortho* isomer is somewhat destabilized in peroxo path **TS3$_{ar}$** compared to the hydroperoxo one **TS2H$_{ar}$**. This suggests that in *ortho* path the alkyl substituent of the arene becomes closer to the POM framework inducing repulsive steric interaction and decreasing its reactivity.

CONCLUSIONS

Three forms of polyanion **1** differing in their protonation state, $[\gamma\text{-}PW_{10}O_{38}V_2(\mu\text{-}O)_2]^{5-}$ (**1**), $[\gamma\text{-}PW_{10}O_{38}V_2(\mu\text{-}O)(\mu\text{-}OH)]^{4-}$ (**1H**) and $[\gamma\text{-}PW_{10}O_{38}V_2(\mu\text{-}OH)_2]^{3-}$ (**1H$_2$**), have been identified by acid-base titration monitored by ^{31}P NMR in MeCN/*t*BuOH solution of TBA-**1H**. The protonation equilibrium constants of **1** and **1H** estimated from the ^{31}P NMR data are equal to $2.5\cdot10^5$ and $8.6\cdot10^3$ M^{-1}, respectively. The kinetic modeling study revealed that hydroperoxo complexes $[\gamma\text{-}PW_{10}O_{38}V_2(\mu\text{-}O)(\mu\text{-}OOH)]^{4-}$ (**2**) and $[\gamma\text{-}PW_{10}O_{38}V_2(\mu\text{-}OH)(\mu\text{-}OOH)]^{3-}$ (**2H**) give a relatively small contribution to the initial rate of PC hydroxylation while peroxo complex $[\gamma\text{-}PW_{10}V_2O_{38}(O_2)]^{3-}$ (**3**) is the most active form of the catalyst and its contribution to the initial

reaction rate is about 70%, although it may depend on the reaction conditions. The DFT calculations also point out that the most active species in the aromatic hydroxylation is the peroxo complex **3**, which in addition can be used to explain the observed regioselectivity further supporting the mechanistic proposal. The preferred positions of oxygen transfer from **3** in the pseudocumene molecule are defined rather by steric than electronic factors. Consequently, unusual regioselectivity toward 2,4,5- and 2,3,5-trimethylphenols results from steric hindrance of the formation of 2,3,6-trimethylphenol via interaction of pseudocumene and **3**. For the studied alkoxy- and alkylarene substrates, anisole and toluene, the selectivity-determining step is also the oxygen transfer from the peroxo complex **3** but, in this case, the observed *para*-hydroxylation regioselectivity is governed by the electronic preference of the substrate.

AUTHOR INFORMATION

Corresponding Author

*Igor Y. Skobelev (email: skobelev@catalysis.ru) and *Jorge J. Carbó (j.carbo@urv.cat)

Author Contributions

The manuscript was written through contributions of all authors. All authors have given approval to the final version of the manuscript.

ACKNOWLEDGMENT

The authors thank Dr. G. M. Maksimov for the synthesis of the lacunary precursor $Cs_7[\gamma\text{-}PW_{10}O_{36}]$. This work was conducted within the framework of the budget project No. 0303-2016-0005 for the Boreskov Institute of Catalysis. The research at Universitat Rovira i Virgili was supported by the Spanish Ministry of Science and Innovation (grant CTQ2014-52774-P), the DGR of the Generalitat de Catalunya (grant2014SGR199 and XRQTC). I.Y.S. acknowledges the

Polyoxometalate Chemistry for Molecular Nanoscience (PoCheMoN) action in the framework of the European Cooperation in Science and Technology (COST) program for financial support.

ASSOCIATED CONTENT

Supporting Information. Additional spectral data, detailed equations of the kinetic modeling, and Cartesian coordinates and absolute energies of computational structures.

REFERENCES

1. *The chemistry of Phenol*, Rappoport, Z., Ed., John Wiley Ltd: Chichester, **2003**.

2. Lorenc, J. F., Lambeth, G., Scheffer, W. In *Kirk-Othmer Encyclopedia of Chemical Technology*, Wiley-VCH: Weinheim, **2003**, Vol. 2, p 203-233.

3. Fiege, H., Voges, H.-W., Hamamoto, T., Umemura, S., Iwata, T., Miki, H., Fujita, Y., Buysch, H.-J., Garbe, D., Paulus, W. In *Ullmann's encyclopedia of industrial chemistry*, Wiley-VCH: Weinheim, **2002**.

4. *The Chemistry of the Quinonoid Compounds*, Patai, S., Rappoport, Z., Eds., Wiley: New York, **1988**.

5. In *The Vitamins*, Schudel, P., Mayer, H., Isler, O., Sebrell, W. H., Harris, R. S., Eds., Academic Press: New York, **1972**, Vol. 5, p 168-217.

6. *Handbook of Vitamins*, Rucker, R. B., Suttie, J. W., McCormick, D. B., Machlin, L. J., Eds., Marcel Dekker: New York, **2001**.

7. Nicolaou, K. C., Chen, J. S., Edmonds, D. J., Estrada, A. A. *Angew. Chem. Int. Ed.* **2009**, *48*, 660-719.

8. O. A. Kholdeeva, O. V. Zalomaeva, *Coord. Chem. Rev.* **2016**, *306*, 302-330.

9. O. A. Kholdeeva, in *Arene Chemistry: Reaction Mechanisms and Methods for Aromatic Compounds*, (Ed.: J. Mortier), Wiley, **2016**, Ch. 14, pp.365-398

10. Lücke, B., Narayana, K. V., Martin, A., Jähnisch, K. *Adv. Synth. Catal.* **2004**, *346*, 1407-1424.

11. Alonso, D. A., Nájera, C., Pastor, I. M., Yus, M. *Chem. Eur. J.* **2010,** *16*, 5274-5284.

12. Enthaler, S., Company, A. *Chem. Soc. Rev.* **2011**, *40*, 4912-4924.

13. Haines, A. H. *Methods for the Oxidation of Organic Compounds: Alkanes, Alkenes, Alkynes and Arenes*, Academic Press: London, **1985**, Vol. 1985.

14. Sheldon, R. A., Arends, I. W. C. E., Hanefeld, U. *Green chemistry and catalysis*, Wiley-VCH: Weinheim, **2007**.

15. Cavani, F., Centi, G., Perathoner, S., Trifirò, F. *Sustainable Industrial Chemistry: Principles, Tools and Industrial Examples*, Wiley-VCH: Weinheim, **2009**.

16. *Liquid phase oxidation via heterogeneous catalysis: organic synthesis and industrial applications*, Clerici, M. G., Kholdeeva, O. A., Eds., Wiley: Hoboken, New Jersey, **2013**.

17. Carril, M., Altmann, P., Drees, M., Bonrath, W., Netscher, T., Schütz, J., Kühn, F. E. *J. Catal.* **2011**, *283*, 55-67.

18. Möller, K., Wienhöfer, G., Westerhaus, F., Junge, K., Beller, M. *Catalysis Today* **2011**, *173*, 68-75.

19. Bonrath, W., Netscher, T. *Appl. Catal. A: Gen.* **2005**, *280*, 55-62.

20. Casani, R. In *Kirk-Othmer Encyclopedia of Chemical Technology*, Wiley-VCH: Weinheim, **2003**, Vol. 25, p 144-150.

21. Asakawa, Y., Matsuda, R., Tori, M., Sono, M. *J. Org. Chem.* **1988**, *53*, 5453-5457.

22. Orita, H., Shimizu, M., Hayakawa, T., Takehira, K. *Bulletin of the Chemical Society of Japan* **1989**, *62*, 1652-1657.

23. Jacob, J., Espenson, J. H. *Inorganica Chimica Acta* **1998**, *270*, 55-59.

24. Carril, M., Altmann, P., Bonrath, W., Netscher, T., Schutz, J., Kuhn, F. E. *Cat. Sci. Technol.* **2012**, *2*, 722-724.

25. C. L. Hill, in *Comprehensive Coordination Chemistry II,* Vol. 4 (Ed.: A. G. Wedd), Elsevier Science, New York, **2004**, pp. 679-759

26. Neumann R. In: *Transition Metals for Organic Synthesis, 2nd Edition,* Vol. 2. Beller M., Bolm C., eds. Wiley-VCH, Weinheim, **2004**, pp. 415-426.

27. Mizuno, K. Kamata, S. Uchida, K. Yamaguchi, in *Modern heterogeneous oxidation catalysis: design, reactions and characterization* (Ed.: N. Mizuno), Wiley-VCH, Weinheim, **2009**, pp 185–217

28. Wang, S.-S., Yang, G.-Y., *Chem. Rev.* **2015**, *115*, 4893-4962.

29. Lechner, M.; Güttel, R.; Streb, C. *Dalton Trans.* **2016**, *45*, 16716-16726.

30. Kamata, K., Yamaura, T., Mizuno, N., *Angew. Chem. Int. Ed.* **2012**, *51*, 7275-7278.

31. Kamata, K., Yonehara, K., Nakagawa, Y., Uehara, K., Mizuno, N., *Nat. Chem.* **2010**, 2, 478-483.

32. I. D. Ivanchikova, N. V. Maksimchuk, R. I. Maksimovskaya, G. M. Maksimov and O. A. Kholdeeva. *ACS Catal.*, **2014**, 4, 2706-2713.

33. Zalomaeva, O. V., Evtushok, V. Y., Maksimov, G. M., Maksimovskaya, R. I., Kholdeeva, O. A. *Dalton Trans.*, **2017**, *46*, 5202-5209.

34. Zalomaeva, O. V., Evtushok, V. Y., Maksimov, G. M., Kholdeeva, O. A. *J. Organomet. Chem.* **2015**, *793*, 210-216.

35. Kamata, K., Sugahara, K., Yonehara, K., Ishimoto, R., Mizuno N., *Chem. Eur. J.* **2011**, 17, 7549 – 7559

36. Nakagawa, Y., Mizuno, N. *Inorg. Chem.* **2007**, *46*, 1727-1736.

37. Kuznetsov, A. E., Geletii, Y. V., Hill, C. L., Morokuma, K., Musaev, D. G. *Inorg. Chem.* **2009**, *48*, 1871-1878.

38. Domaille, P. J., Hervé, G., Téazé, A. In *Inorganic Syntheses*, Ginsberg, A. P., Ed., John Wiley & Sons: **1990**, Vol. 27, p 96-104.

39. Skobelev, I. Y., Zalomaeva, O. V., Kholdeeva, O. A., Poblet, J. M., Carbó, J. J. *Chem. Eur. J.* **2015**, *21*, 14496-14506.

40. *Gaussian 09, Revision C.01*, Frisch, M. J., Trucks, G. W., Schlegel, H. B., Scuseria, G. E., Robb, M. A., Cheeseman, J. R., Scalmani, G., Barone, V., Mennucci, B., Petersson, G. A., Nakatsuji, H., Caricato, M., Li, X., Hratchian, H. P., Izmaylov, A. F., Bloino, J., Zheng, G., Sonnenberg, J. L., Hada, M., Ehara, M., Toyota, K., Fukuda, R., Hasegawa, J., Ishida, M., Nakajima, T., Honda, Y., Kitao, O., Nakai, H., Vreven, T., Montgomery Jr., J. A., Peralta, J. E., Ogliaro, F., Bearpark, M., Heyd, J. J., Brothers, E., Kudin, K. N., Staroverov, V. N., Kobayashi, R., Normand, J., Raghavachari, K., Rendell, A., Burant, J. C., Iyengar, S. S., Tomasi, J., Cossi, M., Rega, N., Millam, J. M., Klene, M., Knox, J. E., Cross, J. B., Bakken, V., Adamo, C., Jaramillo, J., Gomperts, R., Stratmann, R. E., Yazyev, O., Austin, A. J., Cammi, R., Pomelli, C., Ochterski, J. W., Martin, R. L., Morokuma, K., Zakrzewski, V. G., Voth, G. A., Salvador, P., Dannenberg, J. J., Dapprich, S., Daniels, A. D., Farkas, O., Foresman, J. B., Ortiz, J. V., Cioslowski, J., Fox, D. J., Eds., Gaussian Inc.: Wallingford CT, **2010**.

41. Lee, C., Yang, W., Parr, R. G. *Phys. Rev. B* **1988**, *37*, 785-789.

42. Becke, A. D. *J. Chem. Phys.* **1993**, *98*, 5648-5652.

43. Stephens, P. J., Devlin, F. J., Chabalowski, C. F., Frisch, M. J. *J. Phys. Chem.* **1994**, *98*, 11623-11627.

44. Hay, P. J., Wadt, W. R. *J. Chem. Phys.* **1985**, *82*, 299-310.

45. Francl, M. M., Pietro, W. J., Hehre, W. J., Binkley, J. S., Gordon, M. S., DeFrees, D. J., Pople, J. A. *J. Chem. Phys.* **1982**, *77*, 3654-3665.

46. Hehre, W. J., Ditchfield, R., Pople, J. A. *J. Chem. Phys.* **197**2, *56*, 2257-2261.

47. Hariharan, P. C., Pople, J. A. *Theoret. Chim. Acta* **1973**, *28*, 213-222.

48. Jiménez-Lozano, P., Ivanchikova, I. D.; Kholdeeva, O. A.; Poblet, J. M.; Carbó, J. J. *Chem. Commun.* **2012**, *48*, 9266-9268.

49. (a) Schreiber, R. E.; Houben, L.; Wolf, S. G.; Leitus, G.; Lang, Z-L.; Carbó, J. J.; Poblet, J. M.; Neumann, R. *Nat. Chem.*, **2017**, *9*, 369-373; (b) Jiménez-Lozano, P.; Solé-Daura, A.; Wipff, G.; J Poblet, J. M.; Chaumont, A.; Carbó, J. J., *Inorg. Chem.* **2017**, *56*, 4148-4156; (c) Solé-Daura, A.; Goovaerts, V.; Stroobants, K.; Absillis, G.; Jiménez-Lozano, P.; Poblet, J. M.; Hirst, J. D.; Parac-Vogt, T. N.; Carbó, J. J. *Chem. Eur. J.*, **2016**, *22*, 15280-15289; (d) Jiménez-Lozano, P.; Carbó, J. J.; Chaumont, A.; Poblet, J. M.; Rodríguez-Fortea, A.; Wipff, G. *Inorg. Chem.* **2014**, *53*, 778-786.

50. Mammen, M., Shakhovich, E.I., Deutch, J.M., Whitesides, G.M. *J. Org. Chem*. **1998**, *63*, 3821-3830.

51. Domaille, P.J., Harlow, R.L., *J. Am. Chem. Soc.*, **1986**, *108*, 2108-2109.

52. Maksimovskaya, R.I., Subocheva, O.A., Kuznetsova, L.I., *Russ. Chem. Bull. (Engl. Transl.)*, **1986**, *35*, 1977-1986.

53. Kholdeeva, O.A., Maksimovskaya, R.I., *Russ. J. Inorg. Chem. (in Russian)*, **1992**, *31*, 680-683.

54. Derome, A. W. *Modern NMR techniques for chemistry research*, Pergamon: New York, **1987**.

55. de Visser, S.P., Shaik, S.; *J. Am. Chem. Soc*. **2003**, *125*, 7413-7424.

56. Donoeva, B. G.; Trubitsina, T. A.; Antonova, N. S.; Carbó, J. J.; Poblet, J. M.; Kadamany, G. A.; Kortz, U.; Kholdeeva, O. A. *Eur. J. Inorg. Chem.* **2010**, 5312-5317.

57. Jiménez-Lozano, P.; Skobelev, I. Y.; Kholdeeva, O. A.; Poblet, J. M.; Carbó, J. J. *Inorg. Chem.* **2016**, *55*, 6080-6084.

SYNOPSIS TOC